

---

# A Subabdominal MRI Image Segmentation Algorithm Based on Multi-Scale Feature Pyramid Network and Dual Attention Mechanism

Yu Xiao<sup>1</sup>, Xin Yang<sup>2</sup>, Sijuan Huang<sup>2</sup>, Yongkai Liu<sup>3</sup>, Shuqin Chen<sup>4</sup>, Lihua Guo<sup>1</sup>

**Abstract:** This study aimed to solve the semantic gap and misalignment issue between encoding and decoding because of multiple convolutional and pooling operations in U-Net when segmenting subabdominal MRI images during rectal cancer treatment. A MRI Image Segmentation is proposed based on a multi-scale feature pyramid network and dual attention mechanism. Our innovation is the design of two modules: 1) a dilated convolution and multi-scale feature pyramid network are used in the encoding to avoid the semantic gap. 2) a dual attention mechanism is designed to maintain spatial information of U-Net and reduce misalignment. Experiments on a subabdominal MRI image dataset show the proposed method achieves better performance than others methods. In conclusion, a multi-scale feature pyramid network can reduce the semantic gap, and the dual attention mechanism can make an alignment of features between encoding and decoding.

**Keywords:** Biomedical image Segmentation; subabdominal MRI image segmentation; multi-scale feature pyramid network; dual attention; U-Net

## I. Introduction

Medical image segmentation is particularly critical as a prerequisite for relevant quantitative analysis in the treatment of clinical diseases. For example, in clinical cervical cancer radiotherapy, after acquiring subabdominal MRI scans, fast and accurate image segmentation of organs and tumors can optimize the clinical radiotherapy process, whereas traditional approaches use manual annotation by radiation oncologists, which is very time-consuming and laborious. Therefore, an automatic organ segmentation of subabdominal MRI images is a valuable research topic.

In the field of automatic medical image segmentation, U-Net, proposed by Ronneberger et al. [1] in 2015, has achieved remarkable performances. After that,

This work was supported by Guangdong Basic and Applied Basic Research Foundation(2022A1515011549) and (Yu Xiao, Xin Yang and Sijuan Huang have made equal contributions to this work.) (Corresponding author: Lihua Guo, Email: guolihua@scut.edu.cn.)

1. Yu Xiao and Lihua Guo are with the School of Electronic and Information Engineering, South China University of Technology, Guangzhou, Guangdong Province 510641, China.

2. Xin Yang and Sijuan Huang are with the Department of Radiation, Sun Yat-sen University Cancer Center; State Key Laboratory of Oncology in South China; Collaborative Innovation Center for Cancer Medicine; Guangdong Key Laboratory of Nasopharyngeal Carcinoma Diagnosis and Therapy, Guangzhou, Guangdong, 510060, China

3. YongKai Liu is with the Department of radiological sciences, Stanford University, LA, USA.

4. Shuqin Chen is with the Hexiangning College of Art and Design, Zhongkai University of Agriculture and Engineering, Guangzhou, 510225, China.

---

many transformers have been proposed and used U-Net as the backbone network [2-11]. U-Net is a design that allows the features to be reused by the jump connection. It seems that the loss of spatial relationships can be perfectly solved, however, there are still some problems. Firstly, decoding features have some information loss compared with those of encoding, therefore, a semantic gap is still existing there. Secondly, after multiple convolutional and pooling operations, the spatial location and distribution of features have a misalignment problem. Particularly, in the segmentation of subabdominal MRI images, the anal canal and rectum are difficult to be distinguished even for specialist doctors. The main difference between the canal and the rectum is a transition along the internal surface from endodermal to skin-like ectodermal tissue, and it needs rich clinical experience to distinguish. Therefore, the segmentation of subabdominal MRI images is a challenging topic. If spatial relationships of organs do not align, it will cause performance degradation or even failure. Traditional attention methods [8] [12] [13] only compute the similarity between feature points for reinforcing the important features or channels, they could not solve the spatial alignment issue. A new attention mechanism needs to be designed to maintain spatial information. Moreover, the feature pyramid network [14] is a simple and efficient framework for building features pyramids inside the convolutional neural network, and it has been applied in image classification [15], object detection [16], Stereo Matching [17], semantic segmentation [18] and so on. Therefore, the feature pyramid network can be used in the segmentation of subabdominal MRI images for avoiding the semantic gap in U-Net.

Based on these considerations, two modules are proposed in this paper for solving these above problems and suppressing interference from irrelevant regions: 1) Combined with U-Net, a multi-scale feature pyramid network is used in the encoding, and multi-scale features reuse in the decoding process for avoiding the semantic gap. 2) A dual attention mechanism is designed to maintain spatial information of U-Net and reduces misalignment.

## II. Related work

The essence of image segmentation can be seen as the classification of every pixel. Ronneberger et al. [1] proposed a U-Net network for Biomedical Image Segmentation, which consisted of three parts, encoding, decoding, and a jump connection between them. Because of its excellent performance, many network structures based on U-Net have been proposed, such as attention mechanisms, densely connected modules, cascade networks, etc.

Medical images differ from natural images in that they are a set of 3D image slices at different locations. The spacing between slices is usually 1~5mm, so the traditional 2D models have the following problems. Firstly, it is inefficient because 3D data is treated as a series of 2D data. Secondly, valuable spatial information is ignored. To make better use of spatial information, Çiçek et al. [2] proposed a 3D U-Net, which

---

took 3D images as an input and an output, to improve the segmentation accuracy of the U-Net model in 3D images. The V-net [3] has a similar structure to the 3D U-Net, and a residual structure was added to avoid gradient disappearance. The authors used convolution with a step size of two to take place of pooling. When the input image was a 3D image, the corresponding convolution method also changed to 3D convolution, which caused an exponential increment in computational costs. DeepMedic [4] adopted a compromise approach by selecting properly-sized image blocks, and it used full convolution operation to make dense predictions for multiple neighboring pixels, which reduced computational complexity. Due to the regularity of medical images, the selection of image blocks could solve problems of intra-class data imbalance under the control of the scale of the foreground and background. Ibtehaz et al. [5] proposed a MultiRes-UNet method that included the residual path, which allowed the encoder features to perform some additional convolution operations before being fused with the corresponding features in the decoder. These convolution operations were used to balance the depth gap between the sibling encoder and the decoder. Seo et al. [6] argued that traditional jump connection operation was too brutal. For large objects, the dual operations of jump connection and encoding-decoding were repetitive for low-resolution information, and it blurred the boundaries of the segmented target. For small objects, a direct transfer could not effectively learn enough high-resolution features. They proposed the Modified U-Net (mU-Net), which adaptively merged features in the residual path into the jump connection. The FED Net [7] thought that features of different resolutions had semantic differences, and designed feature fusion structures to integrate these features into the encoder. Both mU-Net and FEDnet used convolution in the jump connection to improve the performance of segmentation in medical images. Oktay et al. [8] proposed an attention-gating (AG) system at the end of the jump connection to optimize segmentation by using features of the next level to supervise features of the previous level. This method limited the activation to the region to be segmented, and it reduced the activation value of the background. The authors of Unet++ [9] argued that it was difficult to exactly indicate the number of network layers, so they cleverly made use of the structural features of U-Net to achieve an adaptive selection of the number of network layers. In addition, a series of methods such as MDU-Net [10] and UNet 3+ [11] also achieved the same goal by introducing dense connections. Since 3-D convolutions suffer from high computational costs and GPU memory consumption. Li et al. [19] proposed a hybrid densely connected UNet (H-DenseUNet), which consists of a 2-D Dense U-Net for efficiently extracting intra-slice features and a 3-D counterpart for hierarchically aggregating volumetric contexts.

In the case of segmentation in subabdominal images, especially female pelvic cavity images, there are privacy issues due to the high cost of acquiring medical data. At present, there are not any publicly available datasets on the female pelvic cavity. Li et al. [20] used a small amount of data from six institutions, and proposed a prototype network-based segmentation model to perform segmentation in eight Regions of Interest (ROI) in the male pelvic cavity, including the bladder, rectum, and seminal

---

vesicles. Balagopal et al. [21] used 2D and 3D cascaded U-shaped networks to segment the prostate, bladder, rectum, and femoral head in pelvic cavity CT images. They first used five 2D networks to roughly locate the organs, and then they used five 3D networks to determine the precise location of the organ edges, which was computationally intensive and time-consuming to obtain results. Yang et al. [22] combined CT and MRI for multi-organ segmentation in the male pelvis cavity, and Leonardo et al. [12] fused the squeeze-and-excitation (SE) attention module into U-Net to segment endangered organs of the male pelvis in MRI images from multiple institutions. Another method proposed by Zhang et al. [23] was based on U-Net. It used a multi-scale residual structure to capture remote contextual information, and it segmented multiple organs in the pelvis of men with prostate cancer. To sum up, in the field of subabdominal Image Segmentation, the corresponding datasets are small, and some organs (e.g., anal canal and rectum) are difficult to distinguish in the practical clinical application.

### **III. Subabdominal MRI Image Segmentation**

#### **3.1 Features Reused U-net Network Based on Dilated Convolution and Multi-Scale Feature Pyramid Structure**

This paper proposes features reused U-Net based on dilated convolution and multi-scale feature pyramid structure, which is called Multi-Scale Feature Pyramid Network (MFP-Net) as shown in Figure 1. In the middle of the network, i.e. the pyramid structure, encoding features of different scales are multiplexed through various dilated convolutions with different dilation rates, and features of the same scale are concatenated together. Since more feature multiplexing modules are merged in the decoding process, thus the network gradually enhances the spatial relationship information of the decoding process.

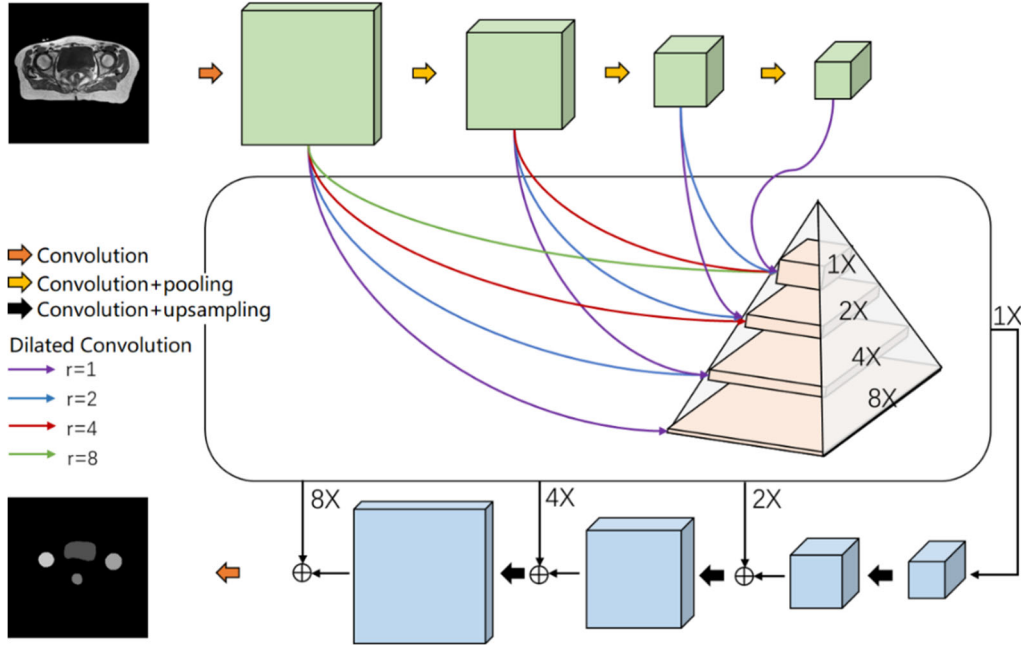


Figure 1 The main framework of the multi-scale feature pyramid network (MFP-Net).

The main improvements of MFP-Net are as follows:

(1) Replacing traditional convolution operation with dilated convolution to achieve the alignment of spatial location relationships in the decoding process. In the proposed network, the input to the decoding layer is not the output of the last encoding layer, but the same size features obtained by dilated convolution from encoded information at different scales with different dilation rates, and they are concatenated together along the channel dimension as the input to the decoding layer. This operation allows the intermediate results of the encoding layer to be reused, and it also allows the high-resolution spatial location relations to be transmitted more directly to the low-resolution layer. The main merit is that the proposed network can enhance spatial representations during decoding, especially by reusing features in the early stages of decoding. In the jump connection, the algorithm replaces the concatenate operation with a point-by-point sum operation, which would reduce the number of parameters, and the residual structure effectively avoids the problem of gradient disappearance.

(2) To extract spatial features, multiple spatial reused structures are used to form a feature pyramid network, which realizes more sufficient feature re-usage and completes the spatial information recovery strategy.

Assuming  $X_E$  and  $X_D$  represent the feature mapping in encoding and decoding respectively,  $X_F$  denotes the feature mapping of the intermediate process. Given input  $I \in R^{1 \times H \times W}$ , the convolutional neural network obtains features  $X_E^i$  at different scales by encoding and pooling for  $i \in (1, 2, \dots, n)$  times, where  $X_E^i \in R^{C_i \times \frac{H}{2^{i-1}} \times \frac{W}{2^{i-1}}}$ . For each  $X_E^i$ , the following operations are performed:

$$X_F^{ik} = D_{r(k)}(H(X_E^{i-1})) \quad k \leq n - i \quad (3)$$

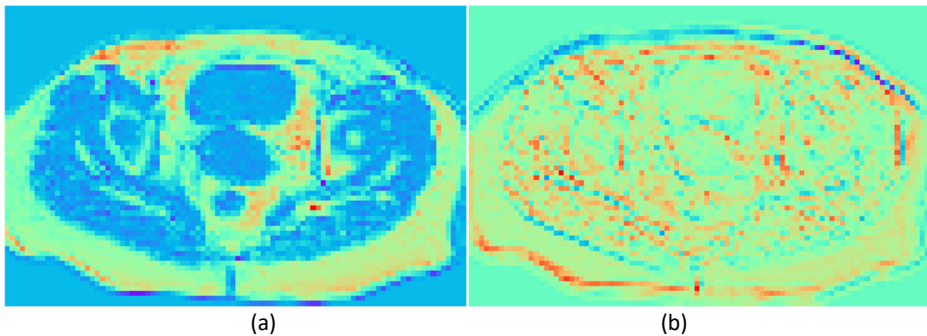
---

where  $D_r(\cdot)$  denotes a dilated convolution with a dilation rate of  $r$ , and  $H(\cdot)$  denotes a single encoding operation.  $X_F^{ik}$  is a set of new features at different scales  $X_F^{ik} = D_{r(k)}(X_i) \in R^{\frac{C_i}{2} \times \frac{H}{r(k)} \times \frac{W}{r(k)}}$ . The input to the decoding network is  $X_D^1 = [X_F^{i1}]$ . The decoding operation can be expressed as:

$$X_D^j = U(H(X_D^{j-1})) + X_F^{ik} \quad (4)$$

Where  $U(\cdot)$  denotes up-sampling,  $X_F^{ik}$  are features from the encoding network, having the same number of channels and resolution as  $U(H(X_D^{i-1}))$ . These improvements leverage the reuse module, and they are helpful for gradually recovering spatial information. In the pyramid structure, not only different scale features are extracted by different dilation rates for scale unified, but also the same scale features are extracted by dilated convolution with different dilation rates, and they are transmitted to decoding at different scales respectively. From another perspective, the reused structure facilitates the fusion of features at different scales in an explicit way, while the decoding network chooses effective information that is more useful for decoding and spatial recovery.

To explain the mechanism of this proposed method, this paper obtains the feature heat maps during the training process, and certain selected maps are shown in Figure 2. Because the spatial position alignment is completed by applying dilated convolution, the four maps have the same resolution. Maps (a), (b), and (c) are the results obtained from a dilated convolution of features with different dilation rates respectively. Map (d) is the decoded feature generated by the corresponding decoding network. It can be observed that the boundary of the image is becoming more and more blurred. In this paper, to allow the decoding feature (d) to recover the spatial relationship information appropriately in advance, features (a) and (b), as well as feature (c), are jointly transmitted to (d) for completing the extraction of spatial relationship and the spatial alignment in one decoding process.



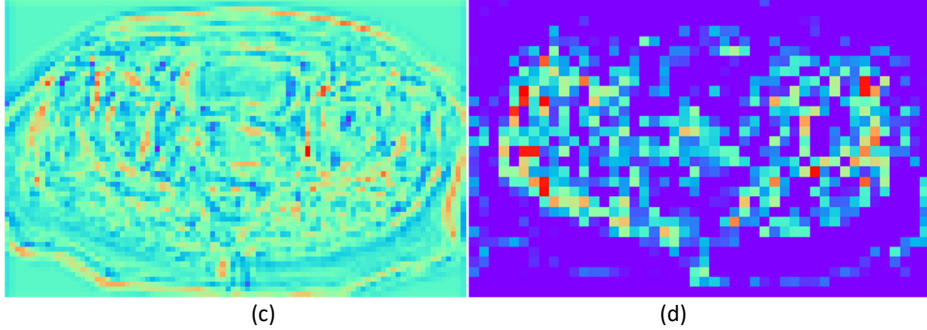


Figure 2 Feature heat maps after dilated convolution, (a) the map after low dilation rate, (b) the map after middle dilation rate, (c) the map after high dilation rate, (d) the decoded feature map from the decoder.

### 3.2 MFP-Net combined with a bi-directional cross-attention mechanism

The bi-directional cross-attention mechanism (BiCA) consists of two aspects: the channel attention mechanism and the spatial attention mechanism, then fuse them. They are described separately as follows.

- **channel attention mechanism**

This method computes channel attention through two input sources. They are encoding features  $O \in R^{C \times H \times W}$  generated in pyramid network and output  $Q \in R^{C \times H \times W}$  in decoding networks, respectively. These two sources are divided into blocks with  $H_0 \times W_0$  size, then calculate their means in each block as follows,

$$S_d^c(X) = \frac{1}{H_0 \times W_0} \sum_{i=dH_0}^{(d+1)H_0} \sum_{j=dW_0}^{(d+1)W_0} X_{ij}^c \quad (5)$$

$S_d^c(X)$  from two input sources are flattened into one dimension as  $g^c(O)$  and  $g^c(Q)$  with  $\left(\frac{H}{H_0} \times \frac{W}{W_0}\right) \times C$  size, and concatenate them together,

$$g^c(M) = [g^c(O), g^c(Q)] \in R^{\left(2 \times \frac{H}{H_0} \times \frac{W}{W_0}\right) \times C \times 1} \quad (6)$$

The mask  $Ma$  can be obtained by learning the channel weight  $L_i$  and applying the formula:

$$Ma = \left[ \sum_{i=1}^{2 \times \frac{H}{H_0} \times \frac{W}{W_0}} L_i g_i^c(M) \right]_c \quad (7)$$

As shown in Figure 3, The module of “get semantic domain” is to calculate the mean of each block by equation 5, and then they are flattened and combined as  $g^c(M)$  by equation 6. The mask  $Ma$  is obtained using 1\*1 convolution of the channel weight  $L$  and  $g^c(M)$  by equation 7. The output of the attention mechanism  $Q'$  is obtained by the dot product of  $Ma$  and output of decoding network  $Q$ , which can be considered as scaling processing. Therefore,  $Q'$  is consistent with  $O$  and  $Q$  in channel dimension, and it can be a Plug-and-play module of the U-Net.

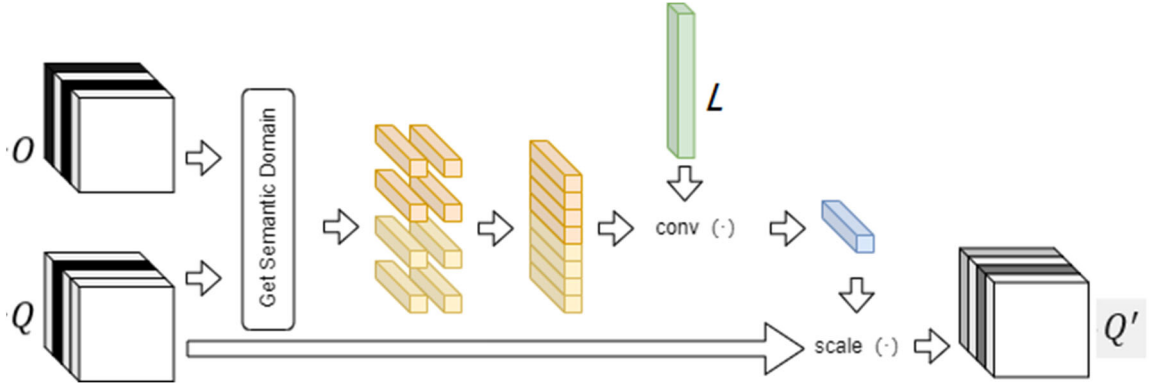


Figure 3. The main framework of the channel attention mechanism based on semantic domain adaptation.

The channel attention mechanism differs from current channel attention modules in two aspects:

1) Conventional channel attention aims to measure the importance of different channels. But the proposed channel attention generates a set of scaling coefficients and applies them to one of the input channels.

2) Most channel attention methods measure the overall features of a channel by global average pooling, which has some shortcomings. Firstly, global averaging pooling does not take the size of the feature map into account, so the mean values vary greatly after different convolution layers. Secondly, the representation capacity of the network is constrained when merely using one weight scalar as the attention of a channel, especially as the attention of a channel with a large resolution size. In our proposed method, the feature channels are divided into blocks with sizes of  $8 \times 8$ ,  $4 \times 4$ ,  $2 \times 2$ , or  $1 \times 1$  for different layers, and the local average pooling can extract the local statistical characters, and further improve the representation capacity of the network.

### ● spatial attention mechanism

Apart from the semantic ambiguity in channels, there is also spatial semantic ambiguity. Due to continuous convolution, downsampling, and upsampling operations, the loss of spatial information mainly comes from the offset of location. The decoding features undergo large offsets with the encoding features, and it naturally results in a misalignment problem when fusing these two features. If the offset can be calculated and corrected, this misalignment problem can be solved.

Inspired by the semantic flow proposed by Li [24], a spatial bias calibration method is proposed in this paper. The bias of flow is calculated between the encoding and decoding features, and the encoding features are calibrated based on the bias of flow, and keep consistency with decoding features. The details of the calculation are as follows:

As shown in Figure 4, features  $O \in R^{C \times H \times W}$  from encoding and features  $Q \in R^{C \times H \times W}$  from decoding are respectively downsampling by  $1 \times 1$  convolution, then concatenated together and parallelly input into two modules with a series of convolutional transformations. After a series of convolutional transformations, the output  $\Delta F \in R^{H \times W \times 2}$  is finally downsampled into two channels. and each channel represents a directional offset. the input features  $O$  is calibrated by following steps:

$$\varphi(O) = G(O, \Delta F + \Delta \xi) \quad (8)$$

where  $\Delta \xi \in R^{H \times W \times 2}$  is the standard offset field whose pixel takes values on a range of  $(-1, -1) \sim (1, 1)$ .  $G$  represents the deformation warp operation, which adjusts input  $O$  to new space according to offset mapping. Warp operation has two steps. Firstly, the positional correspondence of mapping is obtained,

$$G_{h'} = \begin{cases} \min(1, \Delta F_h + \Delta \xi_h) & , \Delta F_h + \Delta \xi_h > 0 \\ \max(-1, \Delta F_h + \Delta \xi_h) & , \Delta F_h + \Delta \xi_h < 0 \end{cases}$$

$$G_{w'} = \begin{cases} \min(1, \Delta F_w + \Delta \xi_w) & , \Delta F_w + \Delta \xi_w > 0 \\ \max(-1, \Delta F_w + \Delta \xi_w) & , \Delta F_w + \Delta \xi_w < 0 \end{cases} \quad (9)$$

Input  $O(h, w)$  is adjusted as  $O(h + G_{h'}, w + G_{w'})$ . Secondly, the new feature  $O'_{h,w}$  is obtained by the bilinear interpolation,

$$O'_{h,w} = \sum_{p \in \tilde{N}} L_p O(h + G_{h'}, w + G_{w'}) \quad (10)$$

where  $\tilde{N}$  represent four neighbor points of  $p$ , and the weight  $L_p$  of each neighbor is assigned by the distance between the neighbor point and the point  $p$ .

The specific structure of the proposed method is shown in Figure 4. Unlike the method proposed by Li [24], the input comes from two features of the same size rather than those of different sizes. In addition, inspired by literature [25], convolution kernels with sizes of  $3 \times 3$  and  $5 \times 5$  are used to enhance the perception of local offsets during the flow calculation.

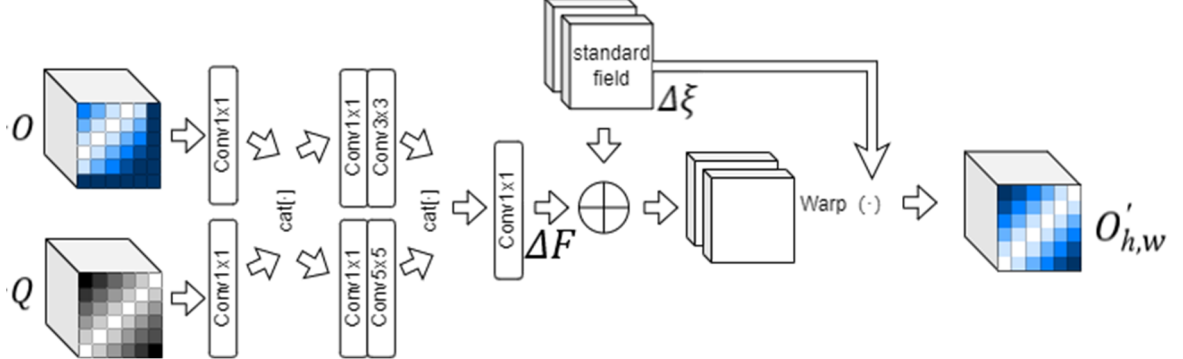


Figure 4. The main framework of the spatial attention mechanism based on semantic flow calibration.

### ● MFP-BiCA-Net with a bidirectional cross-attention mechanism

The two proposed attention mechanisms mentioned above have three common characteristics: Firstly, both have two same input sources and one output result. Secondly, each attention mechanism only calibrates one feature channel, i.e., the encoding feature  $O$  is calibrated by wrapping, and the decoding feature  $Q$  is calibrated by scaling. Thirdly, unlike currently various attention approaches that emphasize calculating the feature attention, the proposed method stresses calibrating the difference between two input sources. The main purpose of these two attention mechanisms is to solve the misalignment problem.

Based on the similarities of the two attention mechanisms, they are merged to

obtain a bidirectional cross-attention network structure, as shown in Figure 5. Bidirectional means dual output from the attention mechanism. The cross comes from the fact that each output utilizes input information from both sources. Features generated via the feature pyramid are passed through the channel attention module, and the features from the decoding layer are passed through the spatial attention module. The results are summed point by point and used as input to the next decoding unit.

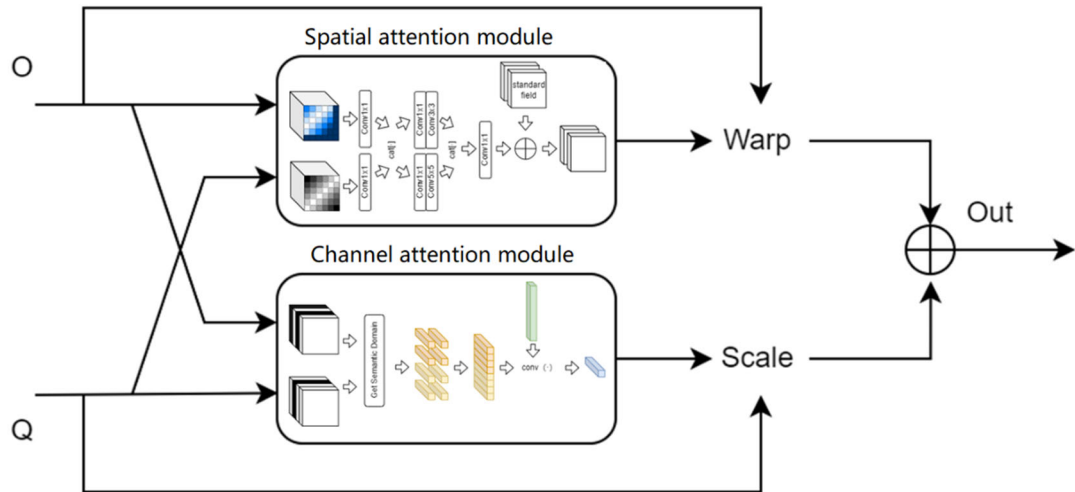


Figure 5. The main framework of bidirectional cross-attention mechanism.

To show the bidirectional cross-attention mechanism directly, feature heat maps are calculated to compare with and without BiCA, as shown in Figure 6. The left column is feature maps that are directly summed without BiCA, and the right column is feature maps that are summed after BiCA. Features in the right column are less jagged due to the neighborhood interpolation algorithm in the spatial attention mechanism, which is highlighted by red circles in the first row. The features of the left are not well aligned compared to those of the right, which are highlighted by red circles in the second row.

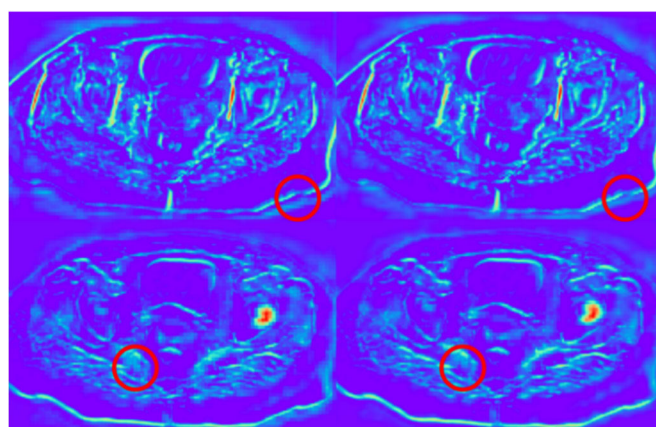


Figure 6. Comparison of feature heat maps. Left column: direct summation, right column: BiCA. Red circles in the first-row point out the jagged problem, and red circles in the second-row point out the alignment problem.

---

## IV. Experiments and results

### 4.1 Dataset and Preprocessing

Our subabdominal MRI image dataset was provided by the cancer center of a local hospital, and all personal-related information had been deleted. To facilitate the subsequent label visualization, the Nibabel library in python was used to parse the raw data (medical DICOM format). Meanwhile, five main organs of the pelvic region were selected for segmentation: the anal canal, bladder, rectum, femoral head (left), and femoral head (right). We divided the study cohort into training (n=55; 66%), validation (n=9; 11%), and testing (n=19; 23%) sets. The image slices were cropped to a matrix size of 256×256 in the central region. The bounding box contained all organ structures in the images. In-fly data augmentation techniques are used, which include rand rotations between  $[-5^\circ, 5^\circ]$ , random contrast adjustment, elastic transformations, and random horizontal flip. We also performed image normalization to reduce skewing.

### 4.2 Experimental parameter settings

Training parameters for the network were as follows: the data were trained in batches with a size of 32, for a total of 400 epochs. The initial learning rate was set to 0.01 and decreased to 0.001 and 0.0001 at the 200th and 300th epoch respectively. SGD was used as an optimizer for the network, setting the momentum term to 0.9 and the weight decay factor to 0.001.

3D deep networks generally performed better than 2D deep networks on medical image segmentation tasks, and a classical 3D medical image segmentation method, H-DenseUNet [19], was selected to test our dataset. Since the GPU memory is 11GB, the batch size can be only 1 for avoiding an overflow of memory in our experimental setting. This method got worse performance than the 2D deep network. The main reason was as follows, the lower the batch size was, the worse performance the deep network achieved. In addition, each slice was one training sample in a 2D network, but the total slice of one patient was one training sample in a 3D network. Therefore, the scale of the training set was bigger in a 2D deep network than that in a 3D deep network. Based on these above reasons, we decided to use 2D networks in our experiments.

### 4.3 Evaluation metrics

Two evaluation metrics are used to evaluate the performance of the model, namely the three-dimensional Dice Coefficient (Volumetric Dice Coefficient, DSC) and the Mean Surface Distance (Mean Surface Distance, MSD). The DSC is used to measure the degree of overlap between two samples and takes values in the range [0,1]. The larger the DSC is, the more similar the two samples are. The MSD is used to measure the physical distance between the samples, and the smaller the MSD is, the closer the samples are to each other. The formula calculating DSC is as follows.

$$DSC = \frac{2|A \cap B|}{|A \cup B|}$$

where A and B are automated and manual 3D segmentations of the organs, respectively. MSD is calculated as follows,

$$MSD(A, B) = \frac{1}{|S(A) + S(B)|} \left( \sum_{a \in S(A)} d(s_a, S(B)) + \sum_{b \in S(B)} d(s_b, S(A)) \right)$$

where  $S(A)$  is the set of surface points in  $A$  and  $S(B)$  is the set of surface points in  $B$ ,  $d(v, S(A)) = \min_{s_a \in S(A)} \|v - s_a\|$ . That is the minimum value of Euclidean distance from this point to all points of another object.

#### 4.4 Analysis of experimental results

For the selection of comparison algorithms, the most popular U-Net structure is chosen first. Since the point-by-point addition is used instead of concatenate operation in the MPF structure, the U-Net with point-by-point addition (U-Net-Add) is added as a baseline method. Some attention methods of U-Net are also selected as comparison algorithms, i.e., UNet++ [9] and r2u-net [26] and a Transformer structure (MedT [30]). To indicate the differences, the method that uses only dilated convolution is named MFP-Net1, while the method using both dilated convolution and multi-scale feature pyramid structures is named MFP-Net2. The significance of differences in DSC and MSD obtained using MFP-Net2 and the baseline UNet-Add method was investigated using a paired sample t-test at the 95% level of confidence.

The model size is added to compare different methods more fairly. The channels of the first convolution operation are 8 channels, 16 channels, and 32 channels respectively, which represent different U-Net structures with different numbers of parameters. The experimental results are shown in Tables 1 and 2 respectively.

Table 1. Number of parameters and Dice coefficients under different network structures (mean  $\pm$  SD)

Network structure	Model size(M)	Anal canal	Bladder	Rectum	femoral head(Left)	femoral head(Right)	Average
UNet-8	2.07	0.628 $\pm$ 0.085	0.888 $\pm$ 0.085	0.761 $\pm$ 0.092	0.903 $\pm$ 0.034	0.908 $\pm$ 0.030	0.8176
UNet-16	8.25	0.639 $\pm$ 0.083	0.894 $\pm$ 0.085	0.766 $\pm$ 0.099	0.916 $\pm$ 0.026	0.919 $\pm$ 0.018	0.8268
UNet-32	32.95	0.652 $\pm$ 0.076	0.891 $\pm$ 0.096	0.775 $\pm$ 0.102	0.920 $\pm$ 0.022	0.920 $\pm$ 0.019	0.8316
UNet++ <sup>[9]</sup>	8.75	0.641 $\pm$ 0.084	0.904 $\pm$ 0.082	0.781 $\pm$ 0.108	0.923 $\pm$ 0.017	0.925 $\pm$ 0.017	0.8348
r2u-net <sup>[26]</sup>	24.35	0.622 $\pm$ 0.081	0.895 $\pm$ 0.082	0.731 $\pm$ 0.118	0.912 $\pm$ 0.018	0.921 $\pm$ 0.015	0.8162
MedT <sup>[30]</sup>	88.59	0.549 $\pm$ 0.088	0.843 $\pm$ 0.089	0.687 $\pm$ 0.111	0.869 $\pm$ 0.030	0.867 $\pm$ 0.027	0.7828
UNet-Add	6.67	0.642 $\pm$ 0.077	0.902 $\pm$ 0.082	0.740 $\pm$ 0.117	0.910 $\pm$ 0.014	0.920 $\pm$ 0.015	0.8228
MFP-Net1	8.09	0.670 $\pm$ 0.076	0.899 $\pm$ 0.088	0.763 $\pm$ 0.112	0.923 $\pm$ 0.021	0.927 $\pm$ 0.014	0.8364
MFP-Net2	8.07	0.668 $\pm$ 0.071 $P > 0.5$	0.905 $\pm$ 0.079 $P > 0.5$	0.773 $\pm$ 0.096 $P < 0.5$	0.924 $\pm$ 0.016 $P < 0.5$	0.924 $\pm$ 0.015 $P > 0.5$	0.8388 $P < 0.5$

Table 2. Model size and MSD for different network structures (in mm)

Network structure	Model size(M)	Anal canal	Bladder	Rectum	femoral head (Left)	femoral head (Right)	Average
U-Net8	2.07	$2.416 \pm 1.812$	$2.652 \pm 4.437$	$1.921 \pm 1.809$	$0.870 \pm 1.009$	$0.469 \pm 0.290$	1.6656
U-Net16	8.25	$1.742 \pm 1.274$	$2.064 \pm 3.744$	$1.342 \pm 1.426$	$0.425 \pm 0.161$	$0.418 \pm 0.132$	1.1982
U-Net32	32.95	$3.403 \pm 7.479$	$2.264 \pm 4.017$	$1.674 \pm 1.454$	$0.407 \pm 0.210$	$0.437 \pm 0.197$	1.6370
UNet++ <sup>[9]</sup>	8.75	$2.875 \pm 5.529$	$1.194 \pm 1.471$	$1.568 \pm 1.540$	$0.435 \pm 0.356$	$0.322 \pm 0.074$	1.2788
r2u-net <sup>[26]</sup>	24.35	$1.995 \pm 2.565$	$2.911 \pm 4.906$	$5.797 \pm 6.888$	$5.035 \pm 7.519$	$1.266 \pm 2.458$	3.4008
MedT <sup>[30]</sup>	88.59	$1.878 \pm 0.682$	$1.273 \pm 0.632$	$2.332 \pm 2.045$	$0.650 \pm 0.219$	$0.322 \pm 0.074$	1.291
UNet-Add	6.67	$1.191 \pm 0.432$	$2.296 \pm 3.973$	$3.486 \pm 5.230$	$1.902 \pm 2.599$	$0.662 \pm 0.499$	1.9074
MFP-Net1	8.09	$1.639 \pm 1.271$	$1.795 \pm 1.703$	$3.308 \pm 4.310$	$0.420 \pm 0.321$	$0.393 \pm 0.225$	1.5110
MFP-Net2	8.07	$1.608 \pm 1.261$ $P < 0.5$	$1.167 \pm 1.685$ $P < 0.5$	$1.556 \pm 1.393$ $P < 0.5$	$0.373 \pm 0.122$ $P < 0.5$	$0.357 \pm 0.115$ $P < 0.5$	$1.0122$ $P < 0.5$

Compared with U-Net in Table 1, it is found that a greater number of parameters does not bring more gain, and a smaller number of parameters also reduces prediction accuracy due to under-fitting. Thus, the algorithm in this paper chooses the U-Net16 structure as the backbone of the network. MFP-Net1 and MFP-Net2 have significantly better prediction results than U-Net16. The spatial multiplex reused structure based on dilated convolution (MFP-Net1) achieves the best Dice coefficient values in the anal canal and femoral head regions (right), with Dice coefficients 3.1% and 0.8% higher than that of U-Net respectively. The pyramidal network (MFP-Net2) achieved the best Dice coefficient values in the bladder and femoral head regions(left), with Dice coefficients 1.7% and 2.1% higher than that of U-Net respectively. MFP-Net has fewer parameters compared to U-Net16 in both the number of parameters and model size, due to the point-by-point summation used in the feature reused structure instead of concatenate, and halves the number of channels in the encoding layer, thus greatly reducing the number of channels in the decoding layer.

As seen in Table 1 and Table 2, MedT applies the Transformer structure to medical image segmentation. It is worth noting that MedT has little improvement on this task, and it needs more than five times the training time, even slower fitting speed, and of course greater memory requirements. Its performance on the Dice coefficient is the worst, but its performance on MSD is not the worst. The reason is that the Transformer structure used by MedT has a strong ability to capture contextual dependencies, and MSD is particularly sensitive to outlier sample points.

Specifically, for each case, box-line plots are used to show the distribution characteristic of statistical data, as shown in Figure 7. Comparing MFP-Net2 with U\_Net16, the boxes of five organs segmentation accuracies are higher using MFP-Net2

than those using U\_Net16, and the outlier points are closer to the box using MFP-Net2 than those using U\_Net16. The results show that MFP-Net2 achieves better performance than U\_Net16.

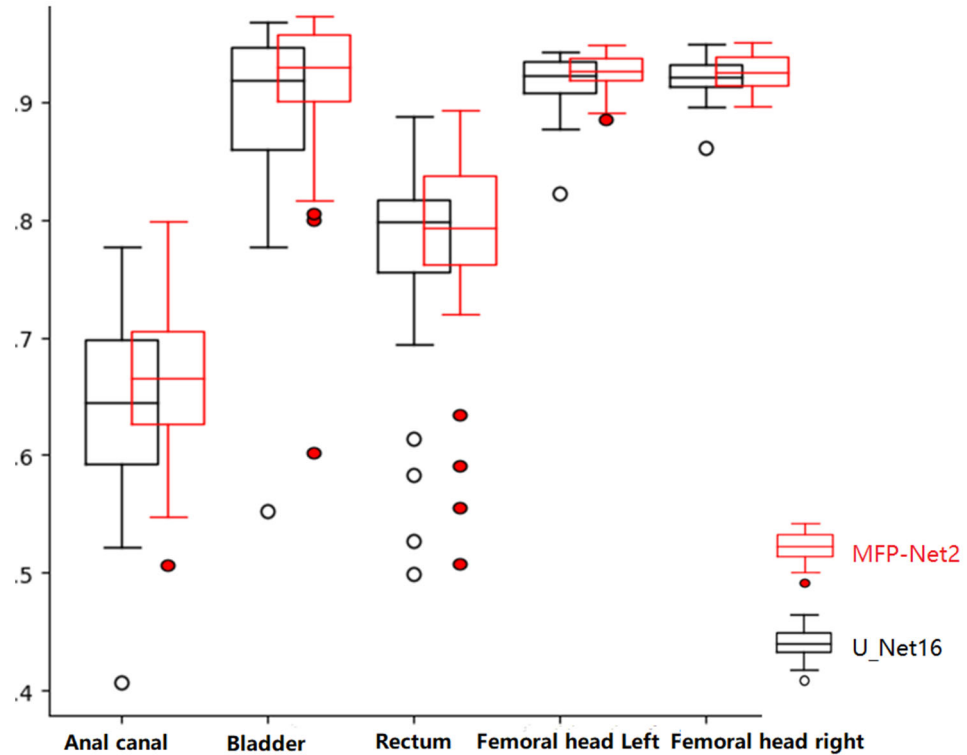


Figure 7. Comparison of the Dice coefficient box-lines of MFP-Net2 and U\_Net

Based on the above analysis, a basic conclusion can be drawn, i.e., the feature reused structure based on dilated convolution and the multi-scale feature pyramid network (MFP-Net) can effectively improve the segmentation performance of organs while using fewer parameters. To present and compare the segmentation results more clearly, the segmentation results of some representative methods are visualized separately in three dimensions from different perspectives, as shown in Figure 8, where different colors represent different organs. It can also be seen that there are isolated prediction points that deviated from the organs in the first three methods, thus causing an increment in false positive values and affecting their DSC. Meanwhile, the more distant the isolated points are, the larger the MSD will be, which leads to the conclusion that a multi-scale feature pyramid network can improve the segmentation performance of organs. It is consistent with the results in Table 2, Table 3, and Figure 3. MedT is insensitive to training boundaries, and it can achieve similar performance when determining whether an organ is present in the slice based on the overall image information, thus it avoids the generation of false positives, Therefore, its deviation points are yet relatively few (it should be noted particularly that due to limitation of video memory, the experiment reduced the size of input images during MedT training, so the jaggedness of segmentation boundary is clear in MedT's visual images), but this learning framework had to be abandoned due to the huge memory requirements of Transformer structure.

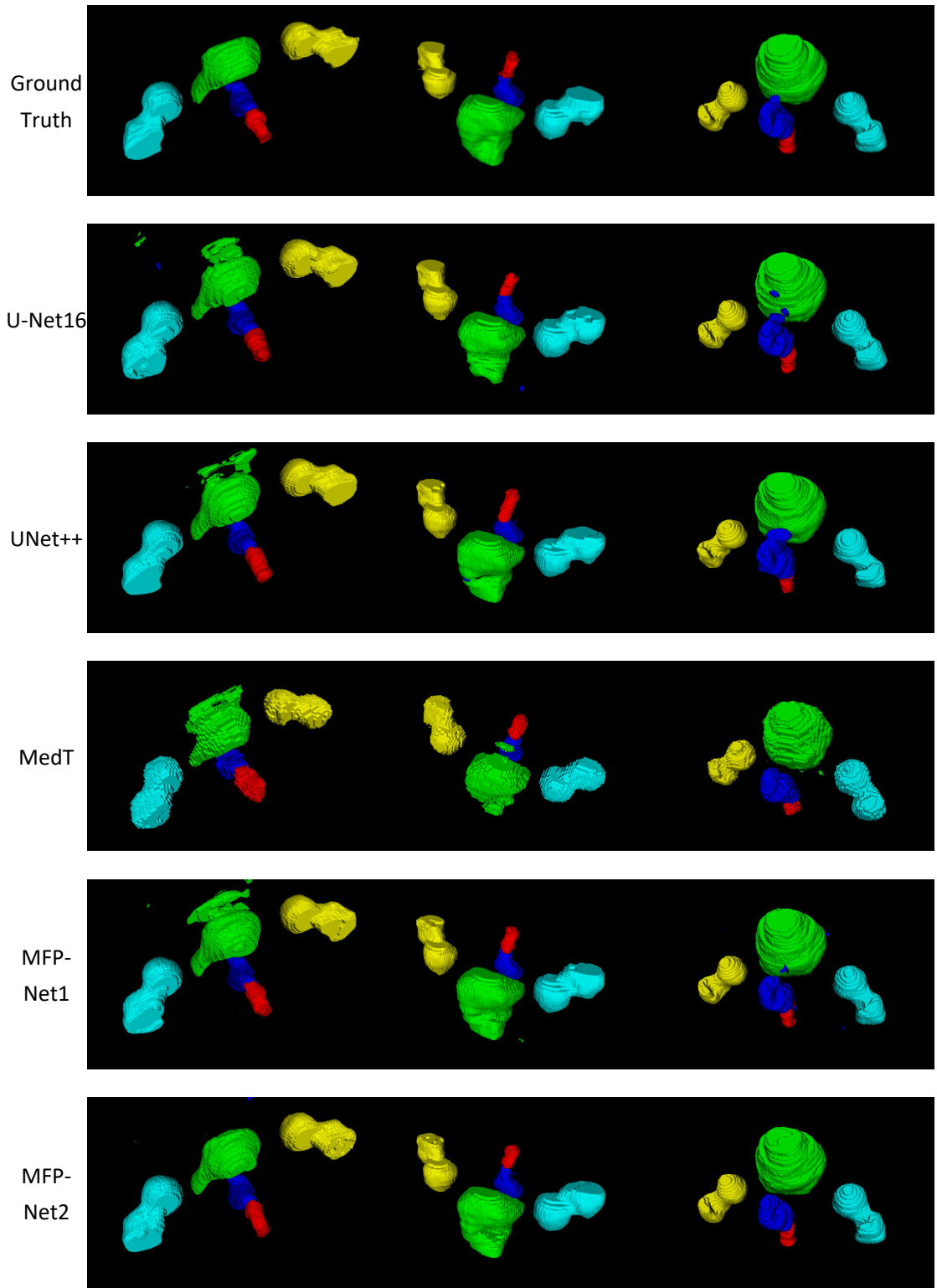


Figure 8. Visualization of the 3D segmentation in different views for different cases. Red - anal canal, dark blue - rectum, yellow and cyan - right and left femoral heads, green - bladder.

We select the MFP-Net as the backbone network and compare our proposed bidirectional cross-attention with other attention methods, i.e., SE [27], GE [28], CBAM [29], and AttentionUnet [30]. Based on MFP-Net, SE structure, GE structure, and CBAM, representatives of channel attention, spatial attention, their combination, and

Attention-Block which used two-channel inputs, are selected and added to jump connection in the same way. In addition, Attention-Block is also added to U-Net (AttentionUNet) for the sake of experimental completeness.

Table 3. Segmentation Dice coefficients for different methods (mean $\pm$ SD)

methods	Anal canal	Bladder	Rectum	femoral head(Left)	femoral head(Right)	Average
MFP	0.668 $\pm$ 0.071	0.905 $\pm$ 0.079	0.773 $\pm$ 0.096	0.924 $\pm$ 0.016	0.924 $\pm$ 0.015	0.8388
MFP+SE <sup>[27]</sup>	0.663 $\pm$ 0.077	0.903 $\pm$ 0.085	0.772 $\pm$ 0.098	0.925 $\pm$ 0.018	0.924 $\pm$ 0.016	0.8374
MFP+GE <sup>[28]</sup>	0.653 $\pm$ 0.079	0.900 $\pm$ 0.085	0.762 $\pm$ 0.108	0.921 $\pm$ 0.025	0.922 $\pm$ 0.015	0.8361
MFP+CBAM <sup>[29]</sup>	0.669 $\pm$ 0.077	<b>0.912<math>\pm</math>0.073</b>	0.773 $\pm$ 0.110	0.921 $\pm$ 0.022	0.926 $\pm$ 0.017	0.8402
MFP+AttBlock	0.665 $\pm$ 0.080	0.908 $\pm$ 0.085	0.781 $\pm$ 0.102	0.925 $\pm$ 0.016	0.926 $\pm$ 0.017	0.8410
AttentionUNet <sup>[30]</sup>	0.642 $\pm$ 0.085	0.908 $\pm$ 0.085	0.781 $\pm$ 0.102	0.925 $\pm$ 0.016	0.926 $\pm$ 0.017	0.8410
MFP+BiCA	<b>0.678<math>\pm</math>0.075</b>	0.906 $\pm$ 0.084	<b>0.785<math>\pm</math>0.095</b>	<b>0.928<math>\pm</math>0.019</b>	<b>0.929<math>\pm</math>0.015</b>	<b>0.8452</b>

It can be seen from Table 3 that the proposed method based on a bidirectional cross-attention mechanism was able to achieve better performances on the MFP network framework, with better results for each organ compared to the initial MFP network. Compared to other attention methods, the combination of MFP and BiCA achieved the best Dice coefficient values at the anal canal, rectum, femoral head(left), and femoral head(right), with 0.9% exceeding the previous best score in segmentation of anal canal. One of the difficulties in the experiment is the segmentation of the anal canal, which has a small size and ambiguous boundaries. BiCA was proposed to solve the problem of ambiguous boundaries caused by semantic ambiguity, which is greatly magnified in smaller organs. In conclusion, the method based on a bidirectional cross-attention mechanism can effectively alleviate the feature mismatch problem caused by multi-resolution feature aggregation, and solve the ambiguity generated in jumping connections, improving the ability to segment regional boundaries.

As 3D visualization can only display overall prediction performance, a visualized comparison is performed on 2D outlined contours, and the results are shown in Figure 9. The proposed method has more outstanding performance on the edge contours of organs, compared to existing attention mechanisms. It is due to the differential discrimination of feature maps by the BiCA module, which is consistent with the conclusions in Table 4.

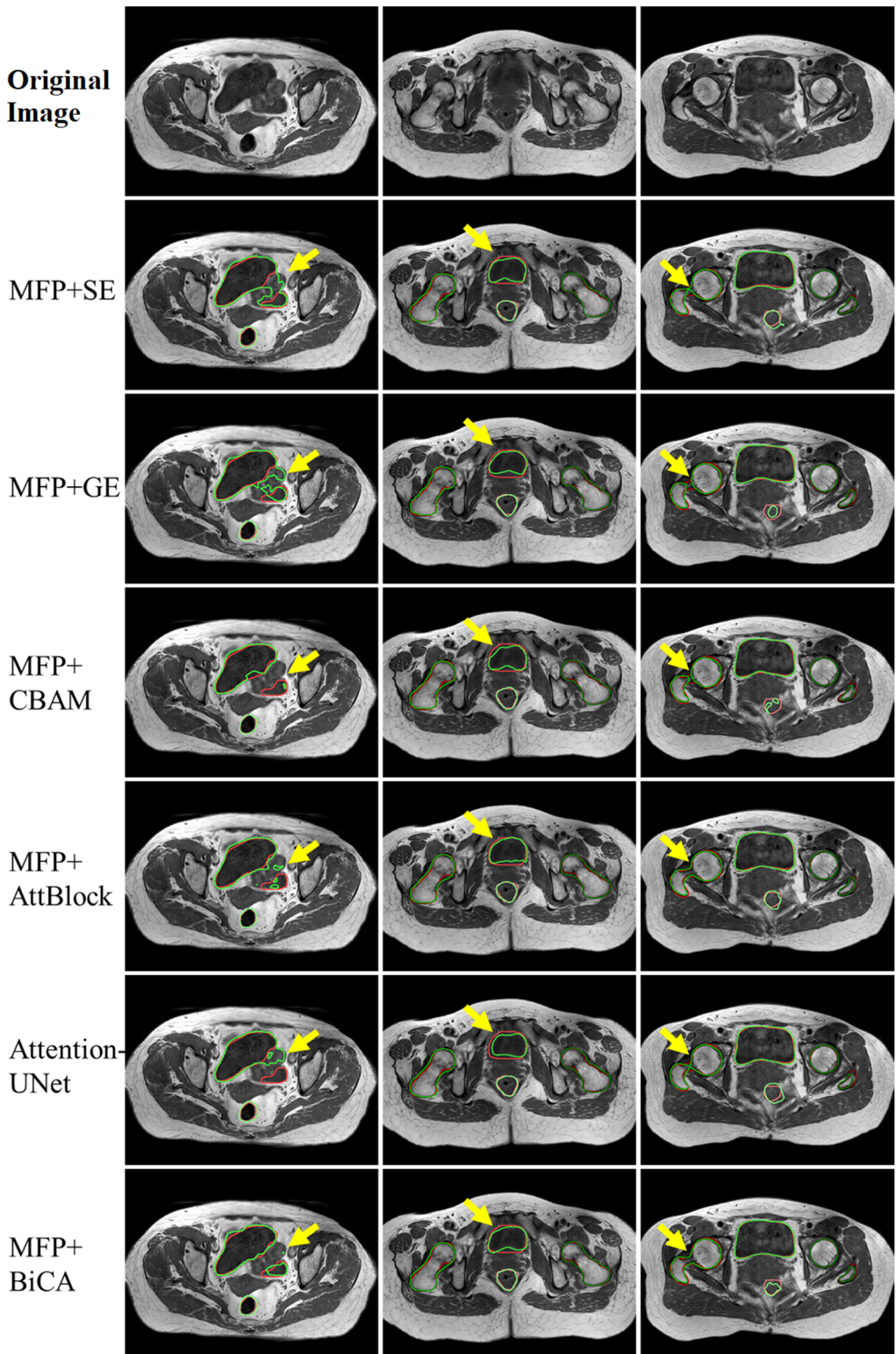


Figure 9. Slice segmentation results. The red contour is the label, and the green contour is the prediction of different methods. The yellow arrows point to the areas where the difference in error is more significant.

## V. Conclusions

Based on the analysis of shortcomings in traditional encoder-decoder network

---

structure, i.e., jump connections are not able to convey strong constraints on the recovery of spatial relationship information, especially during decoding. Two methods are proposed in this paper for improvement, 1) Combined with U-Net, dilated convolution and multi-scale feature pyramid networks are used in the encoding, and multi-scale features reuse in the decoding for avoiding the semantic gap. 2) A dual attention mechanism is designed to maintain spatial information and reduces the misalignment problem. The feature-reused structure utilizes the large-scale receptive field of dilated convolution to sequentially extract new features, and this structure fuses these new features to obtain input features to the decoding network with stronger spatial information. The multi-scale feature pyramid network fuses corresponding reused features before each decoding, which maximizes the spatial information recovery on the decoding network. The dual attention mechanism corrects channel and spatial deviations between encoding and decoding, enabling them to complete spatial alignment before merging. Experimental results show that the proposed network can significantly reduce the false positive problem, and achieves better performance than others methods.

## References

- [1] Ronneberger O., Fischer P., Brox T. U-Net: Convolutional Networks for Biomedical Image Segmentation. International Conference on Medical Image Computing and Computer-Assisted Intervention. Berlin Heidelberg: Springer, 2015: 234-241.
- [2] Çiçek Ö., Abdulkadir A., Lienkamp S.S., et al. 3D U-Net: learning dense volumetric segmentation from sparse annotation. International conference on medical image computing and computer-assisted intervention. Cham: Springer, 2016: 424-432.
- [3] Milletari F., Navab N., Ahmadi S.A. V-net: Fully convolutional neural networks for volumetric medical image segmentation. 2016 fourth international conference on 3D vision (3DV). IEEE, 2016: 565-571.
- [4] He K., Zhang X., Ren S., et al. Deep residual learning for image recognition. Proceedings of the IEEE conference on computer vision and pattern recognition. IEEE, 2016: 770-778.
- [5] Ibtehaz N., Rahman M.S. MultiResUNet: Rethinking the U-Net architecture for multimodal biomedical image segmentation. Neural Networks, 2020, 121: 74-87.
- [6] Seo H., Huang C., Bassenne M., et al. Modified U-Net (mU-Net) with incorporation of object-dependent high level features for improved liver and liver-tumor segmentation in CT images. IEEE transactions on medical imaging, 2019, 39(5): 1316-1325.
- [7] Chen X., Zhang R., Yan P. Feature fusion encoder decoder network for automatic liver lesion segmentation. 2019 IEEE 16th international symposium on biomedical imaging (ISBI 2019). IEEE, 2019: 430-433.
- [8] Oktay O., Schlemper J., Folgoc L., et al. Attention U-Net: Learning where to look for the pancreas. arXiv preprint arXiv, 2018:1804.03999.
- [9] Zhou Z., Siddiquee M., Tajbakhsh N., et al. Unet++: Redesigning skip connections to exploit multiscale features in image segmentation. IEEE transactions on medical imaging, 2019, 39(6): 1856-1867.
- [10] Zhang J., Jin Y., Xu J., et al. MDU-Net: Multi-scale Densely Connected U-Net for biomedical image segmentation. arXiv preprint arXiv, 2018:1812.00352
- [11] Huang H., Lin L., Tong R., et al. UNet 3+: A full-scale connected UNet for medical image segmentation. ICASSP 2020-2020 IEEE International Conference on Acoustics, Speech and Signal Processing (ICASSP).

---

IEEE, 2020: 1055-1059.

[12] Leonardo R., Han C., Yudai N., et al. Use-net: Incorporating squeeze-and-excitation blocks into u-net for prostate zonal segmentation of multi-institutional MRI datasets. *Neurocomputing*. 2019, 365:31-43.

[13] Wang X., Girshick R., Gupta A., et al. Non-local neural networks. *Proceedings of the IEEE conference on computer vision and pattern recognition*. IEEE, 2018: 7794-7803.

[14] Lin T., Dollár P., Girshick R., et al. Feature pyramid networks for object detection. *Proceedings of the IEEE conference on computer vision and pattern recognition*. 2017: 2117-2125.

[15] Chen C., Fan Q., Panda R. Crossvit: Cross-attention multi-scale vision transformer for image classification. *Proceedings of the IEEE/CVF international conference on computer vision*. 2021: 357-366.

[16] Guo W., Li W., Gong W., et al. Extended feature pyramid network with adaptive scale training strategy and anchors for object detection in aerial images. *Remote Sensing*, 2020, 12(5): 784.

[17] Zhu Z., He M., Dai Y., et al. Multi-scale cross-form pyramid network for stereo matching. 2019 14th IEEE Conference on Industrial Electronics and Applications (ICIEA). IEEE, 2019: 1789-1794.

[18] Ku T., Yang Q., Zhang H. Multilevel feature fusion dilated convolutional network for semantic segmentation. *International Journal of Advanced Robotic Systems*, 2021, 18(2), doi:10.1177/17298814211007665.

[19] Li X. et al., “H-DenseUNet: hybrid densely connected UNet for liver and tumor segmentation from CT volumes,” *IEEE Transactions on Medical Imaging*, 2018, 37(12):2663-2674.

[20] Li Y., Fu Y., Yang Q., et al. Few-shot image segmentation for cross-institution male pelvic organs using registration-assisted prototypical learning. *arXiv preprint arXiv*, 2022: 2201.06358.

[21] Balagopal A., Kazemifar S., Dan N., et al. Fully automated organ segmentation in male pelvic CT images. *Physics in Medicine and Biology*, 2018, 63(24).

[22] Yang L., Tonghe W., Sibo T., et al. Male pelvic multi-organ segmentation aided by CBCT-based synthetic MRI. *Physics in Medicine and Biology*. 2020, 65(3).

[23] Zhang Z., Zhao T., Gay H., et al. ARPM-net: A novel CNN-based adversarial method with Markov random field enhancement for prostate and organs at risk segmentation in pelvic CT images. *Medical Physics*, 2021, 48(1):227-237.

[24] Li X., You A., Zhu Z., et al. Semantic flow for fast and accurate scene parsing. *European Conference on Computer Vision*. Cham: Springer, 2020: 775-793.

[25] Szegedy C., Liu W., Jia Y., et al. Going Deeper with Convolutions. *IEEE Conference on Computer Vision and Pattern Recognition*. IEEE, 2015:1-9.

[26] Alom M., Hasan M., Yakopcic C., et al. Recurrent residual convolutional neural network based on u-net (r2u-net) for medical image segmentation. *arXiv preprint arXiv*, 2018: 1802.06955.

[27] Hu J., Shen L., Sun G. Squeeze-and-excitation networks. *Proceedings of the IEEE conference on computer vision and pattern recognition*. IEEE, 2018: 7132-7141.

[28] Hu J., Shen L., Albanie S., et al. Gather-Excite: Exploiting feature context in convolutional neural networks. *Advances in Neural Information Processing Systems*. 2018: 9401-9411.

[29] Woo S., Park J., Lee J.Y, et al. Cbam: Convolutional block attention module. *Proceedings of the European conference on computer vision (ECCV)*. 2018: 3-19.

[30] Valanarasu J., Oza P., Hacihaliloglu I., et al. Medical Transformer: Gated Axial-Attention for Medical Image Segmentation. *International Conference on Medical Image Computing and Computer-Assisted Intervention*. Cham: Springer, 2021: 36-46.